Heliyon 10 (2024) e24346

Contents lists available at ScienceDirect

Heliyon

journal homepage: www.cell.com/heliyon

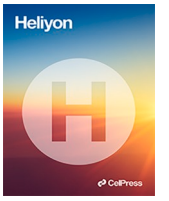

Research article

Screen-printed electrode designed with MXene/doped-polyindole and MWCNT/doped-polyindole for chronoamperometric enzymatic glucose sensor

Katesara Phasuksom **, Nuttha Ariyasajjamongkol, Anuvat Sirivat *

Conductive and Electroactive Polymers Research Unit, The Petroleum and Petrochemical College, Chulalongkorn University, Bangkok, 10330, Thailand

ARTICLE INFO

Keywords:
MXenes
Conductive polymers
Multi-walled carbon nanotubes
Composites
Glucose biosensor
Electrochemistry

ABSTRACT

The enzymatic glucose sensors as modified by MXene-dPIn and MWCNT-dPIn on a screen-printed carbon electrode (SPCE) were investigated. Herein, MXene was molybdenum carbide (Mo_3C_2) which has never been utilized and reported for glucose sensors. The biopolymer type to support the enzyme immobilization was examined and compared between chitosan (CHI) and κ-carrageenan (κC). MWCNT-dPIn obviously showed a larger electroactive surface area, lower charge transfer resistance and higher redox current than Mo_3C_2-dPIn, indicating that MWCNT-dPIn is superior to Mo_3C_2-dPIn. For the chitosan-based sensors, the sensitivity value of CHI-GOD/Mo_3C_2-dPIn is 3.53 μA mM^{-1} cm^{-2} in the linear range of 2.5–10 mM with the calculated LOD of 1.57 mM. The sensitivity value of CHI-GOD/MWCNT-dPIn is 18.85 μA mM^{-1} cm^{-2} in the linear range of 0.5–25 mM with the calculated LOD of 0.115 mM. For the κ-carrageenan based sensors, κC-GOD/MWCNT-dPIn exhibits the sensitivity of 15.80 μA mM^{-1} cm^{-2} and the widest linear range from 0.1 to 50 mM with the calculated LOD of 0.03 mM. The presently fabricated sensors exhibit excellent reproducibility, good selectivity, high stability, and disposal use. The fabricated glucose sensors are potential as practical glucose sensors as the detectable glucose ranges well cover the glucose levels found in blood, urine, and sweat for both healthy people and diabetic patients.

1. Introduction

The glucose level in the blood is extremely vital for diabetes as it is related to various health issues such as lethargy, strokes, blindness, numbness, kidney failure, and heart attacks [1]. The excessive glucose level in the blood called hyperglycemia causes thirst, rapid heartbeat, vision problems, vomiting, tiredness, and rapid heartbeat, whereas the low blood glucose level called hypoglycemia involves sweating, headache, confusion, blurred vision, and lack of coordination [1]. Hence, the real blood glucose level is essential for a diabetes diagnosis to reduce the disease severity. For healthy people, the blood glucose level is 4.0–5.4 mM in fasting and 7.8 mM in postprandial periods. For prediabetes, the blood glucose level is 5.5–6.9 in fasting and 7.8–11.0 mM in postprandial periods. For diabetes, the blood glucose level is over 7 mM in fasting and more than 11.1 mM in postprandial periods [2]. The glucose level in blood is well correlated with the glucose levels in urine and sweat, which are found in lower levels when compared to blood. The glucose

* Corresponding author.
** Corresponding author.
E-mail addresses: pkatesara.p@outlook.com (K. Phasuksom), anuvat.s@chula.ac.th (A. Sirivat).

https://doi.org/10.1016/j.heliyon.2024.e24346
Received 6 November 2023; Received in revised form 6 December 2023; Accepted 8 January 2024
Available online 12 January 2024

concentration found in urine is between 2.78 and 5.55 mM for normal people and above 5.55 mM for diabetes, whereas the glucose concentration ranges in sweat are 0.06–0.11 mM for normal people and 0.01–1 mM for diabetes [3].

Recently, electrochemical biosensors are the most often used owing to the ease of use and maintenance, low cost, high sensitivity, and good repeatability [4,5]; they are suitable as the point-of-care devices relative to other methods namely the surface plasmon resonance (SPR), HPLC, spectrophotometry, fluorescence, and chemiluminescence [6]. Modification of biosensor on a screen-printed electrode, containing the three electrodes (working electrode, reference electrode, and counter electrode) of the electrochemical cell, is widely pursued and commercially marketed because of low cost, ease of use for the on-site analysis, miniaturization, requirement of a small volume of analyst, portability, mass production, and disposal analysis for healthcare devices [7,8]. The commercially available glucose sensors as produced by major companies (namely Abbot, Bayer, Johnson & Johnson, and Roche Diagnostics) are mostly designed to be based on the screen-printed electrode with disposable use as electrochemical enzymatic glucose sensors [9]. The enzymatic glucose sensor is preferable as a point-of-care device because of its high accuracy, selectivity, simplicity, and relative affordability [6]. The mechanism of the enzymatic glucose sensor, as proposed by Clark and Lyon, is based on the idea that glucose is oxidized to gluconolactone by glucose oxidase (GOD) in the presence of oxygen and generate hydrogen peroxide (H_2O_2) [10,11]. Oxygen consumption and H_2O_2 generation are indirectly correlated to glucose concentration [10,12]. Glucose oxidase is a common enzyme for the glucose detection because of its low cost, high bioactivity, and high selectivity to glucose.

To improve the performances of a glucose sensor, the electrode modification with conductive polymers is promising as it facilitates the glucose oxidase immobilization and the electron transfer from the enzymatic reaction [10]. The outstanding properties of conductive polymers are tunable optical and electrical properties, compatibility with biological molecules, and simple attachment on the electrode surface by electrochemical polymerization or drop coating [13,14]. Conductive polymers that have been used in glucose sensors were polyaniline [10], polythiophene [15], polypyrrole [16,17], polycarbazole [18], poly (azure A) [19], and polyindole [14, 20]. Polyindole is one of the tunable conductive polymers, its structure comprises of pyrrolytic ring connected with benzene ring. It is a good candidate for biosensors because of stable redox activity, low cost, facile synthesis, stable doped-state in air, and low toxicity [21, 22]. However, the electrical conductivity of polyindole is lower than other conducting polymers such as polyaniline, poly (3,4-ethylenedioxythiophene), and polypyrrole [22]. Thus, a conductive polymer composite/hybrid is an alternative approach to improve the electrical conductivity, enzyme immobilization, electron transfer ability, and electrocatalytic activity resulting in the higher sensitivity and lower limit of detection for biosensors [23,24].

Herein, the focused materials for the composite/hybrid with polyindole are multi-walled carbon nanotube (MWCNT) and MXenes. MWCNT is a stack of graphene layers rolled up into concentric cylinders, its advantages are large surface area, excellent conductivity, and good biocompatibility, rendering it suitable for electrochemical biosensors [25]. Moreover, it can improve the electrocatalytic activity of glucose oxidase and electron transfer between redox site of enzyme and electrode surface, electroactive surface area, and sensor sensitivity [26]. Mxenes are a novel 2D material with a few layers of transition metal carbides, nitride, or carbonides. MXenes are of the formal formula of $M_{n+1}X_nT_x$ as obtained by etching layers of Al from bulk M_{n+1}-AX_n phase where M is one of the transition metals namely Ti, Cr, Ta, Nb, Mo, and Hf, A is one of *sp* elements (group 13 and 14), and X represents either C or N atom [27,28]. The remarkable properties of Mxenes, namely the high electrical conductivity, biocompatibility, high electrochemical activity and a large surface area, are suitable towards electrochemical biosensor applications [27,29]. MXene modified glucose sensors and other analytical biosensors that have been reported used Ti_3C_2 [30,31]. Mo_3C_2 is a MXene with superior electrical conductivity: its resistivity at room temperature is about 1.0×10^{-6} Ω m [32]; its catalytic behavior is induced by their tunable surface and structure and electronic features; it can be quite resistant towards oxidation and corrosion [33]. Mo_3C_2 has been reported as well in supercapacitors and electrochemical ion detectors [34]. However, Mo_3C_2 has not been previously reported in glucose sensor applications.

Biopolymers provide variously desired properties such as non-toxicity, biodegradability, biocompatibility and high affinity to proteins, rendering them suitable supports for enzymes. Furthermore, the reactive functional groups in their structures such as hydroxyl, amine, and carbonyl groups provide direct reactions with the enzymes and facilitate the modification of sensor surface [35]. Chitosan is a natural polysaccharide; its structure consists of amino and hydroxyl groups suitable for biological binding and interaction with nanomaterials [36]. Chitosan behaves as a polycationic polymer via the protonation of amino groups at low pH; the amino group of chitosan is protonated when pH < pKa (pKa of chitosan is 6.5) [37]. Its advantages are biocompatibility, non-toxicity, low cost, good film formation, and ease in chemical modifications due to the presence of reactive amino and hydroxyl functional groups [38]. Chitosan is a simply added biological element which can be easily coated/electrodeposited on a sensor surface [36]. κ-Carrageenan is a polyanionic polymer due to the sulfate groups on its structure. It can be used as a suitable support material for the enzyme immobilization to improve the stability, activity, and reusability of enzymes [39]. Previous works reported GOD encapsulated in a polyelectrolyte complex (PEC) of chitosan/κ-carrageenan through the electrostatic interaction between glucose oxidase and PEC as glucose sensors [40,41]; GOD possessed the negative charged surface at a physiological condition (pH between 7.35 and 7.45), whereas GOD exhibited the positive charged region of the positive charged lysine residues [42]. However, no previous report exists on the comparison between chitosan-GOD and κ-carrageenan-GOD as a glucose sensor.

Therefore, the first aim of this work is to fabricate a chronoamperometric enzymatic glucose sensor on SPCE by the modifications along with the comparison between MWCNT/doped-PIn and MXene/doped-PIn. Herein, Mo_3C_2 is a MXene type which has not been previously reported as a glucose sensor. The second aim is the comparison of the immobilizations of GOD by a polycationic polymer (chitosan) and a polyanionic polymer (κ-carrageenan) as the support materials through the electrostatic interactions with GOD.

2. Materials and methods

2.1. Materials and reagents

Glucose oxidase enzyme (GOD, 248,878 U/g) of type VII from aspergillus niger was obtained from Sigma-Aldrich and stored at −20 °C prior to use. D Glucose anhydrous was received from Carlo Erba. Indole monomer and ferric chloride were obtained from Merck and perchloric acid was purchased from Panreac. Chitosan (M_w 190,000–310,000 Da), κ-Carrageenan sulfated plant polysaccharide (M_w 672,000 Da [43]), and sodium hydroxide (NaOH) were purchased from Sigma-Aldrich. Glutamic acid was received from TCI. MWCNT (length ~ 15 μm, outer dimension 30–50 nm, >95 % purity) was received from AlphaNano Technology Co., Ltd. Mo_3C_2 MXene powder was obtained from Nanochemazone, Canada. SPCE on polycarbonate (Product's code: CI1703OR; dimensions of 12.5 × 30 mm (width × length)), with the working electrode area of 0.07 cm^2, were purchased from Quasense Co., Ltd., Thailand. The SPCE consists of triple electrodes namely a working electrode, a counter electrode, and a reference electrode made of carbon mixed graphite, carbon, and silver/silver chloride (Ag/AgCl), respectively. A phosphate buffer solution (PBS, pH 7.4) was prepared using sodium phosphate monobasic and sodium phosphate dibasic as purchased from Sigma-Aldrich. Potassium hexacyanoferrate (II) and (III) with 99 % of purity, $K_3[Fe(CN)_6]/K_4[Fe(CN)_6]$ were purchased from Sigma-Aldrich, and potassium chloride (KCl) was obtained from Merck. Ethanol and hydrochloric acid and ethanol were obtained from RCI Labscan. All reagents were of analytical grades.

2.2. Polyindole synthesis

Polyindole (PIn) was synthesized by oxidative polymerization following the previous work [44]. Indole monomer (3.0 g) was dissolved in 10 mL of ethanol. Then, the indole monomer solution was slowly added into the oxidant solution (10.33 g of ferric chloride dissolved in 180 mL distilled water). Next, the mixture was stirred at 26 °C for 24 h. PIn was precipitated in 0.1 M HCl and then filtered by a Buchner funnel and a Whatman filter paper no. 42. The precipitate was rinsed with deionized water several times and then dried at 70 °C for 24 h to obtain a clean PIn precipitate. The PIn precipitate was mildly ground by a mortar to prepare a PIn powder. Next, the PIn in a powder form was de-doped with 5 mol/L ammonium hydroxide (NH_4OH) at the indole: NH_4OH mole ratio of 1:10. The de-doped solution was stirred for 24 h and then filtered and rinsed by deionized water. The de-doped PIn was dried at 70 °C. In the doping process, the de-doped polyindole (dPIn) was doped with 2.5 mol/L perchloric acid ($HClO_4$) at the indole: $HClO_4$ mole ratio of 1:10 for 24 h, and then filtered and rinsed by deionized water. The doped dPIn powder was dried at 70 °C overnight.

2.3. Preparation of composite solution

10 mg of MWCNT was dispersed in 1 mL ethylene glycol by an ultrasonic bath for 1 h and stirred at room temperature for 2 days. 10 mg Mo_3C_2 MXene was dispersed in 1 mL propylene glycol by the ultrasonic bath for 1 h and stirred at room temperature for 2 days. The dPIn powder (20 mg) was dissolved ethylene glycol (1 mL) for 24 h at room temperature without sonication. Each MWCNT solution and Mo_3C_2 solution was mixed with the dPIn solution at the volume ratio of 1:1, and consequently stirred at room temperature for 24 h to obtain the composite solutions. The composite solutions were stirred to obtain the homogeneous solutions prior to use.

2.4. Electrode modification

4 μL of the composite solution was drop coated on the SPCE working electrode and dried at 70 °C for 2 h 5 μL of biopolymer-GOD solution namely chitosan mixed GOD (CHI-GOD) or κ-carrageenan mixed (κC-GOD) was drop coated on the working electrode. To prepare a biopolymer-GOD solution, 5 mg/mL of GOD in PBS was mixed with 1%w/v of biopolymer solution at the volume ratio of 1:2.0.5 % w/v glutamic acid in distilled water acting as a cross linker was used as a solvent for the biopolymer. Then, the enzyme immobilized electrode was dried for 2 h at room temperature and then stored at 4 °C in a vacuum seal bag prior to use. The chitosan-

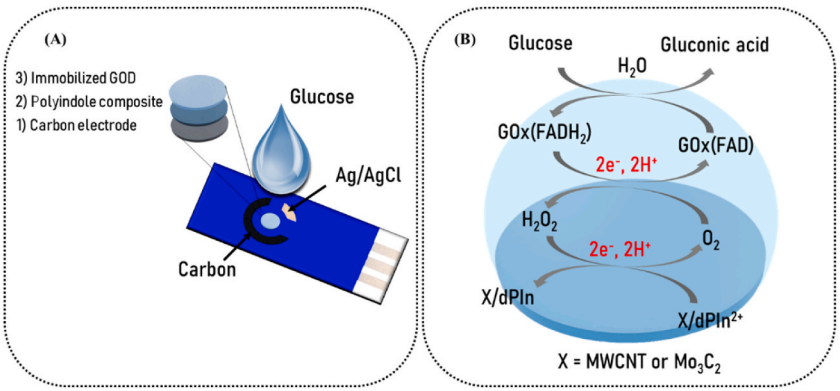

Scheme 1. (A) Modification of SPCE and (B) glucose sensor mechanism.

GOD immobilized on MWCNT-dPIn and Mo_3C_2 were coded as CHI-GOD/MWCNT-dPIn and CHI-GOD/Mo_3C_2-dPIn, respectively. κ-carrageenan-GOD modified on MWCNT-dPIn was coded as κC-GOD/MWCNT-dPIn. The electrode modification step is illustrated in Scheme 1(A).

2.5. Characterization

A FTIR spectrometer (Nicolet™ iS™5, Thermo Scientific™) ATR mode was used to verify the functional groups of the modified electrodes. The wavenumber range was between 650 and 4000 cm^{-1} with 64 cm^{-1} resolution and 64 scans. An XPS spectrometer (Axis Ultra DLD, Kratos Analytical Shimadzu Group Company) was used to analyze the atomic elements and chemical bonding. XPS wide scans and high-resolution scans were recorded by using the pass energies of 160 eV and 40 eV with a standard Al Kα X-ray radiation source. C 1s at the binding energy 248.8 eV was used as a reference. XPS survey and high-resolution spectra were analyzed by a Casa-XPS software. A field emission scanning electron microscope, FE-SEM (HITACHI, S-4800), was used to identify the surface morphology of the modified electrodes with a beam current of 10 mA and an acceleration voltage of 5 kV. The samples for FE-SEM were sputter coated with platinum prior to use.

2.6. Electrochemical measurements

Cyclic voltammetry was operated in an electrolyte solution containing 5 mM of $K_3[Fe(CN)_6]/K_4$ $[Fe(CN)_6]$ and 0.1 M PBS (pH 7.4) in 0.1 M KCl to investigate electrochemical properties of the modified electrodes and to determine the electroactive surface area [16]. The scan rate was varied between 10 and 70 mV/s, and the potential applied was between −1.0 and + 1.0 V with the potential step of 20 mV. To investigate the mechanism of glucose sensors, the modified electrodes were tested in the 10 mM glucose solution by cyclic voltammetry. The potential applied was from −0.8 to 0.8 V with the scan rates from 10 to 60 mV/s. To determine glucose responses in several glucose concentrations, chronoamperometry was carried out at +0.6V vs Ag/AgCl within 400 s. The electrochemical cell was incubated in glucose solutions for 3 min before applying a constant potential to the electrochemical system [14]. The glucose solution (pH 7.4)was prepared a in 0.1 M PBS solution and stored at room temperature for 24 h before use to obtain equilibrium mutarotation between the α and β forms of D-glucose [45]. Electrochemical impedance spectroscopy (EIS) was operated in a 5 mM of K_3 $[Fe(CN)_6]/K_4[Fe(CN)_6]$ solution containing 0.1 M PBS and 0.1 M KCl from 10^{-1} to 10^6 Hz with an amplitude of 10 mV. The electrochemical experiment was carried out with PalmSens4 (PalmSens Instruments BV, the Netherlands) with the PSTrace 5.9 software. The electrochemical and analytical parameters are summarized in Tables S1–S2.

3. Results and discussion

3.1. Characterization of the modified electrodes

The functional groups of the modified electrodes were investigated by ATR-FTIR. The SPCE shows the peaks at 3350 cm^{-1}, 2849-2976 cm^{-1}, and 1078 cm^{-1} corresponding to the O–H stretching, C–H stretching, and C–O stretching, respectively, as shown in Fig. S1. The Mo_3C_2-dPIn shows the characteristic peaks of the dPIn at 3284, 1571, and 738 cm^{-1} corresponding to the N–H stretching, N–H deformation, and out of plane C–H deformation of benzene ring, respectively [14], as well as the stretching of benzene ring at 1617, 1455, 1214 cm^{-1} [44]. The strong absorbance band at 1078 cm^{-1} is attributed to the dopant ClO_4^- [44]. Two peaks at 3523 and 3564 cm^{-1} appear when Mo_3C_2 was composited with dPIn which may be related to the characteristic peaks of Mo_3C_2. The CHI-GOD/Mo_3C_2-dPIn reveals the characteristic peaks of CHI-GOD at 3370, 3271, 1651, 1550, and 1081 cm^{-1}, corresponding to the O–H stretching, N–H stretching, amide I (stretching of C═O of amide linkage), amide II (bending of N–H of amide linkage), and C–O stretching, respectively [46] as shown in Fig. S2.

Some of IR peaks of the CHI-GOD/MWCNT-dPIn are shifted to higher wavenumbers when compared to CHI/MWCNT-dPIn and GOD indicating the intermolecular hydrogen bonding interaction between GOD and CHI [47]. Moreover, the increases of amide I and amide II signals compared to CHI/Mo_3C_2-dPIn can confirm the interaction between GOD and CHI [47]. The MWCNT-dPIn presents the N–H stretching at 3265 cm^{-1}, the Cl–O stretching of the dopant ClO_4^- at 1057 cm^{-1}, and the N–H deformation at 1534 cm^{-1} derived as the fingerprints of the dPIn [44]. Other IR peaks of the asymmetric and symmetric stretching of CH_2 at 2850 cm^{-1} and 2925 cm^{-1}, C═C stretching at 1646 cm^{-1} appear as the fingerprints of MWCNT [48]. The CHI-GOD/MWCNT-dPIn shows the presence of CHI-GOD at 3373, 3286, 1646, 1547, 1074 cm^{-1} which can be assigned to the O–H stretching, N–H stretching, amide I, amide II, and C–O stretching, respectively [46] as shown in Fig. S3. The intermolecular hydrogen bonding interaction between GOD and CHI is confirmed by the shifts of N–H stretching, amide I and amide II to higher wavenumbers when compared to CHI/MWCNT and GOD, and by the increases of amide I and amide II signals when compared to CHI/MWCNT/dPIn [47].

The IR peaks of κC-GOD/MWCNT-dPIn can be observed in Fig. S4. The IR peaks at 3430, 3291, 1642, 1538 cm^{-1} can be attributed to the O–H stretching, N–H stretching, amide I, and amide II, respectively [47,49]. Other IR peaks of the sulfate stretching at 1419 cm^{-1}, the O═S═O asymmetric stretching at 1236 cm^{-1}, the glycosidic linkage at 1070 and 1042 cm^{-1}, the C–O–C stretching at 926 cm^{-1} are related to κC [49]. Some of IR peaks shift to higher wavenumbers when compared to κC/MWCNT-dPIn and GOD as a result of the hydrogen bonding interaction [47]. A new IR peak of amide II appears indicating the successful κC-GOD immobilization. Another reason of the IR shifting found in both CHI-GOD/MWCNT-dPIn and κC-GOD/MWCNT-dPIn maybe related to the electrostatic interaction between the biopolymers and GOD [50]. Generally, GOD shows a negative charge at a physiological condition, which can interact with the positive charge (-NH_3^+) of CHI (polycationic polymer), whereas the positive charge of lysine residues of GOD can

possibly interact with the negative charge (-OSO_3^-) of κC (polyanionic polymer) [42].

The element contents at each modification step were analyzed by XPS and listed in Table S3. Element contents of the SPCE are carbon, oxygen, chlorine, and silicon. The presence of silicon as a contaminant and the existence of chloride in SPCE imply the components of a carbon ink used [14]. After the SPCE was coated with Mo_3C_2-dPIn, the XPS spectrum shows the new elements of molybdenum and nitrogen which can be attributed to MO_3C_2 and dPIn, respectively. The CHI-GOD immobilized on Mo_3C_2-dPIn is confirmed by the increases in atomic percentages of nitrogen and oxygen, in which both are the major elements in the functional groups of both CHI and GOD. The amount of molybdenum decreases resulting from the CHI-GOD layer covering the Mo_3C_2-dPIn layer. For the coating of MWCNT-dPIn on the SPCE, the XPS spectrum shows the new element of nitrogen as derived from the dPIn incorporated in MWCNT. For CHI-GOD/MWCNT-dPIn, the XPS spectrum exhibits the increases in O and N resulting from the functional groups in CHI and GOD. For κC-GOD/MWCNT-dPIn, the XPS spectrum shows the increases in oxygen and nitrogen, and the new element of S emerges which can be attributed to the existence of κC-GOD immobilized on MWCNT-dPIn. The presence of sodium after immobilization is derived from PBS used as the solvent for GOD.

Morphological surfaces of the modified electrode were examined by FE-SEM as shown in Fig. 1. The SPCE working electrode surface shows some carbon nanoparticles mixed with graphene flakes as presented in Fig. 1(a) [14]. Mo_3C_2-dPIn shows the incorporation of dPIn and Mo_3C_2 particles as shown in Fig. 1(b). However, the Mo_3C_2 and Mo_3C_2-dPIn surfaces are different. Some Mo_3C_2 particles are not covered by dPIn particles possibly indicating that Mo_3C_2 is not compatible with dPIn as can be clearly observed from Fig. S5 (a and b). The MWCNT-dPIn surface demonstrates good compatibility between MWCNT and dPIn as shown in Fig. 1(c); MWCNT and dPIn

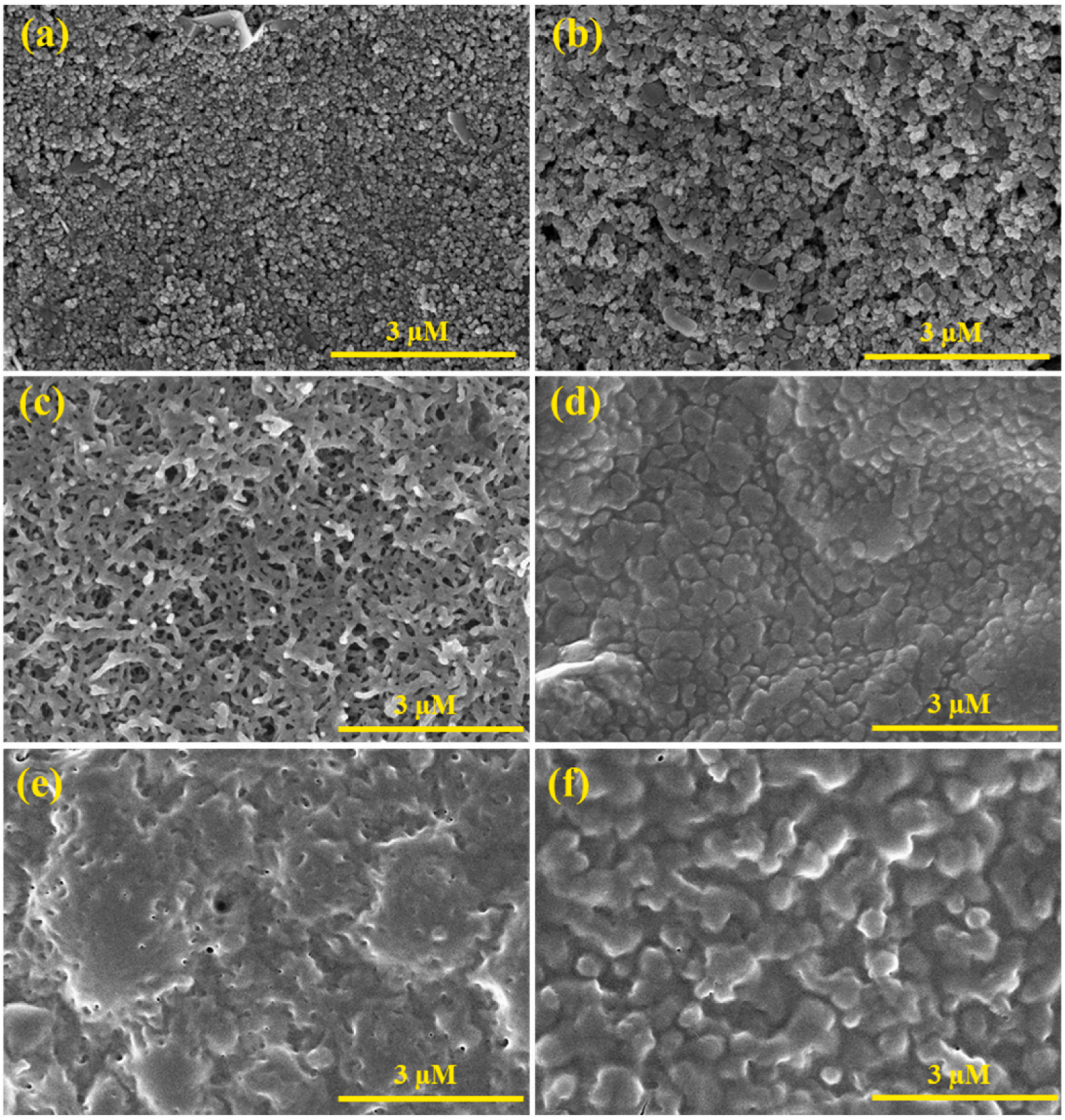

Fig. 1. Morphological surfaces at 15,000 magnification of: (a) SPCE; (b) Mo_3C_2-dPIn; (c) MWCNT-dPIn; (d) CHI-GOD/Mo_3C_2-dPIn; (e) CHI-GOD/MWCNT-dPIn; and (f) κC-GOD/MWCNT-dPIn.

interact by the π-π interaction between aromatic rings [14]. MWCNT is completely covered with dPIn with the porous structure. The pristine MWCNT is compared to MWCNT-dPIn as shown in Fig. S5 (c and d). It is apparent that the fiber shape of MWCNT-dPIn is different from the pristine MWCNT as dPIn perfectly covers the MWCNT fibers. GOD immobilized on the composite layer is illustrated in Fig. 1(d)–(f). The morphological surface of biopolymer-GOD is different as it depends on the biopolymer type. κC-GOD/MWCNT-dPIn possesses a more surface roughness than CHI-GOD/MWCNT-dPIn. Another reason is the difference of composite surface before the immobilization, CHI-GOD/MWCNT-dPIn provides a smoother surface than CHI-GOD/Mo_3C_2-dPIn.

3.2. Electrochemical measurement

Electrochemical behavior of each modified electrode was investigated by cyclic voltammetry in a 5 mM $K_3[Fe(CN)_6]/K_4[Fe(CN)_6]$ solution containing 0.1 M PBS and 0.1 M KCl at the 50 mV/s scan rate as shown in Fig. 2. The anodic and cathodic current responses of the Mo_3C_2/MWCNT and the MWCNT-dPIn are higher than SPCE, implying that these two composites provide the higher electron transfer between the electrode and the electrolyte as well as the higher surface area than SPCE [51]. The MWCNT-dPIn obviously demonstrates the higher anodic and cathodic current response than the Mo_3C_2-dPIn because MWCNT-dPIn provides the higher electrical conductivity than Mo_3C_2-dPIn and the good compatibility of MWCNT and dPIn can also enhance the electron transfer rate and electrochemical performance through the π-π interaction between dPIn and MWCNT [16,52]. Furthermore, the composite modified SPCE provides a beneficial increase in electroactive surface area over bare SPCE leading to the higher redox reaction. The MWCNT-dPIn provides a larger electroactive surface area than Mo_3C_2-dPIn, as will be confirmed in the later step. The ratios of anodic/cathodic peak currents (I_{pa}/I_{pc}) for the $[Fe(CN)_6]^{3-/4-}$ redox probes of SPCE, Mo_3C_2-dPIn, MWCNT-dPIn are 1.05, 2.62, 1.92, respectively. The values of peak-to-peak separation ($\Delta E_p = E_{pa}\text{-}E_{pc}$) for SPCE, Mo_3C_2-dPIn, MWCNT-dPIn are 199 mV, 400 mV, and 460 mV, respectively. Theoretically, the reversible reaction suggests that ΔE_p is 59 mV, and I_{pa}/I_{pa} is equal to 1 [53]. In the case of $I_{pa}/I_{pc} > 1.5$, it becomes a quasi-reversible reaction [54]. Thus, I_{pa}/I_{pa} and ΔE_p values of SPCE, Mo_3C_2-dPIn, and MWCNT are larger than the theoretical values; it can be suggested that they are related to the quasi-reversible reaction. After the immobilization of GOD, the anodic and cathodic current responses decrease; the anodic potential shifts to a more positive value whereas cathodic potential shifts to more negative value. ΔE_p values of GOD-CHI/Mo_3C_2-dPIn, CHI-GOD/MWCNT-dPIn, and κC-GOD/MWCNT-dPIn are 560 mV, 580 mV, and 560 mV, respectively. This clearly shows that ΔE_p of the κC-GOD/MWCNT-dPIn ($\Delta E_p = 560$ mV) is 2.8 times larger than that of SPCE ($\Delta E_p = 199$ mV) indicating the higher energy required to generate the redox reaction of the redox probe $[Fe(CN)_6]^{3-/4-}$. In addition, the anodic and cathodic peak currents of the κC-GOD/MWCNT-dPIn ($I_{pa} = 263.5$ μA and $I_{pc} = -93.1$ μA) are higher than those of SPCE ($I_{pa} = 81.1$ μA and $I_{pc} = -77.5$ μA) implying that the electrical conductivity of the modified electrode was improved. The results of CV are consistent with the SPCE modified with a composite of CNTs-gold nanoparticles [55], and the SPE modified with a composite of PPy-AuNPs [56]. The increase of ΔE_p after the GOD immobilization indicates the slower electron transfer as a result of the non-electrical layers of both CHI-GOD and κC-GOD increasing the electrode resistance [57]. The clear cyclic voltammograms are separately reported in Fig. S6 in Supplementary Materials.

The charge transfer resistance (R_{ct}) at electrolyte/electrode interface was investigated by EIS using $[Fe(CN)_6]^{3-/4-}$ as a redox probe in the 0.1 M KCl and 0.1 M PBS solutions. The Nyquist plots of the various modified electrodes are exhibited in Fig. 3(a). A semicircle at high frequency is attributed to the electron transfer limited process and the straight line at low frequency is referred to the diffusional process [58]. SPCE is visibly observed as the full semicircle with R_{ct} of 1800 Ω as shown in Fig. 3(b), indicating a low electron transfer of the redox probe at the electrolyte/electrode interface. The modified SPCEs demonstrates a partial semicircle at high frequency. Therefore, the evaluation of R_{ct} of MWCNT-dPIn and Mo_3C_2-dPIn before and after GOD immobilization is illustrated in Fig. 3(c) and (d), respectively. The R_{ct} values of the MWCNT-dPIn, the CHI-GOD/MWCNT-dPIn, and the κC–CHI–GOD/MWCNT-dPIn are 75 Ω, 100 Ω, and 130 Ω, respectively whereas that of the Mo_3C_2-dPIn is 900 Ω. The R_{ct} values of MWCNT-dPIn and Mo_3C_2-dPIn are still lower than SPCE indicating that the composites possess the higher electrical conductivity for the electrode fast charge transfer [59].

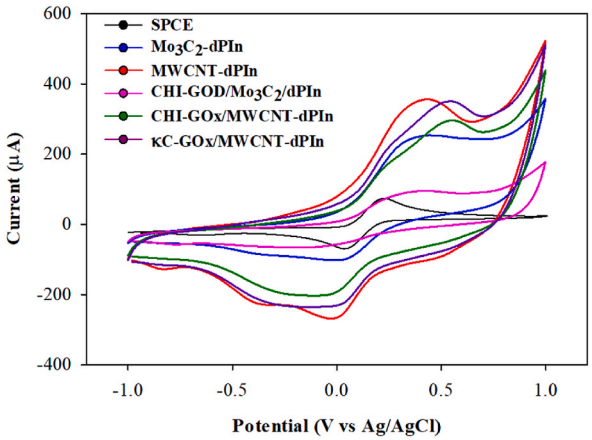

Fig. 2. Cyclic voltammograms of various modified electrodes in 5 mM K_3 $[FeCN_6]/K_4$ $[FeCN_6]$ solution containing 0.1 M PBS and 0.1 M KCl.

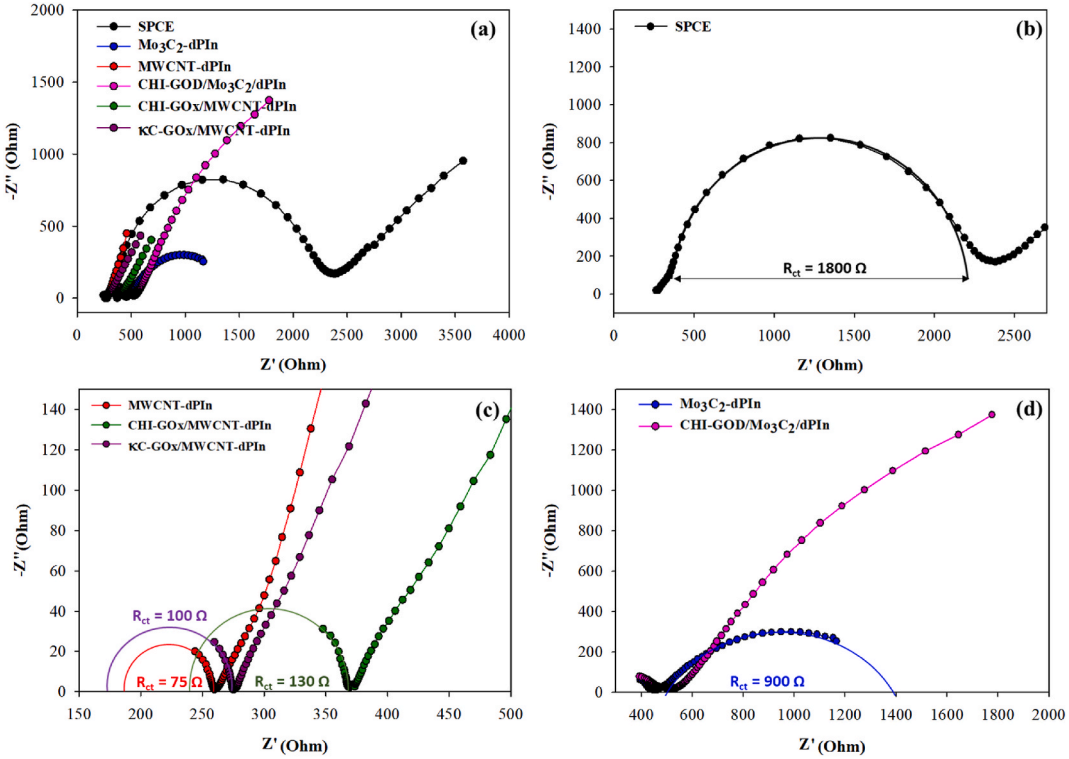

Fig. 3. Nyquist plots of: (a) various modified electrodes; and (b)–(d) estimation of the charge transfer resistance (R_{ct}) of each modified electrode.

However, the R_{ct} of the Mo_3C_2-dPIn is higher than MWCNT, implying a lower electrical conductivity. After the CHI-GOD immobilization, the R_{ct} value increases because of the insulator nature of enzyme and biopolymers obstructing the $[Fe(CN)_6]^{3-/4-}$ transfer to the electrolyte/electrode interface. The semicircle of the CHI-GOD/Mo_3C_2-dPIn appears to be larger as can be observed in Fig. 3(d).

3.3. Electroactive surface area

The electroactive surface area of the fabricated electrodes was investigated under the reaction between $[Fe(CN)_6]^{3-}$ and $[Fe(CN)_6]^{4-}$ by cyclic voltammetry at various scan rates. The cyclic voltammograms of the Mo_3C_2-dPIn and the MWCNT-dPIn at various scan rates and the relation of anodic current response and square root scan rates are depicted in Fig. S7. The electroactive surface area can be calculated by the Randles-Sevcik as shown in equation (1) [18,60]. The slope of I vs $\nu^{0.5}$ was used for the calculation. After substitution of the constant values, the electroactive surface area is correlated with the slope (I vs $\nu^{0.5}$) as shown in equation (2).

$$I = 0.4463(F^3/RT)^{0.5} A_e n^{0.5} D^{0.5} C_0 \nu^{0.5} \quad (1)$$

$$A_e = 2.71 \times 10^{-4} \times \text{slope (I vs } \nu^{0.5}) \quad (2)$$

where I is the current signal (reduction or oxidation) (μA), A_e is the electroactive surface area (cm^2), F is the Faraday constant (96,485 C/mol), T is the absolute temperature (298 K), R is the gas constant (8.314 J/mol·K), n is the number of transferred electrons in redox reaction (n = 1 for $[Fe(CN)_6]^{3-}/[Fe(CN)_6]^{4-}$), D is the diffusion coefficient ($D = 7.6 \times 10^{-6}$ cm^2/s for $[Fe(CN)_6]^{3-}$redox probe system) [61], C_0 is the redox probe concentration (5 mM), and ν is the scan rate (V/s). The electroactive surface areas of the Mo_3C_2-dPIn and the MWCNT-dPIn are 31.3 mm^2, 54.0 mm^2, respectively, which are higher than that of the bare SPCE (8.81 mm^2) [14]. The MWCNT-dPIn provides the larger electroactive surface area than the Mo_3C_2-dPIn because of the porous structure of the MWCNT-dPIn. The large electroactive surface area provides more enzyme immobilization sites leading to a greater enzymatic reaction toward glucose [62]. After the immobilization of GOD, the cyclic voltammograms of the CHI-GOD/Mo_3C_2-dPIn, the CHI-GOD/MWCNT-dPIn, and the κC-GOD/MWCNT-dPIn at various scan rates are presented in Fig. 4 (a-c) and the relation of anodic current responses and square root scan rates are depicted in Fig. 4(d). Anodic peak potential positively shifts and cathodic potential negatively shifts with the increase of scan rates which can be associated with a slow transfer of electrons at the interface [63]. The electroactive surface areas of CHI-GOD/Mo_3C-dPIn$_2$, CHI-GOD/MWCNT-dPIn, and κC-GOD/MWCNT-dPIn as calculated by Randles–Sevcik equation (1) are 14.6 mm^2, 39.9 mm^2, and 49.9 mm^2, respectively. The electroactive surface area is reduced after the enzyme immobilization because the surfaces became smoother [64]. The R_{ct} values and electroactive surface areas of the modified SPCEs are summarized in Table S4.

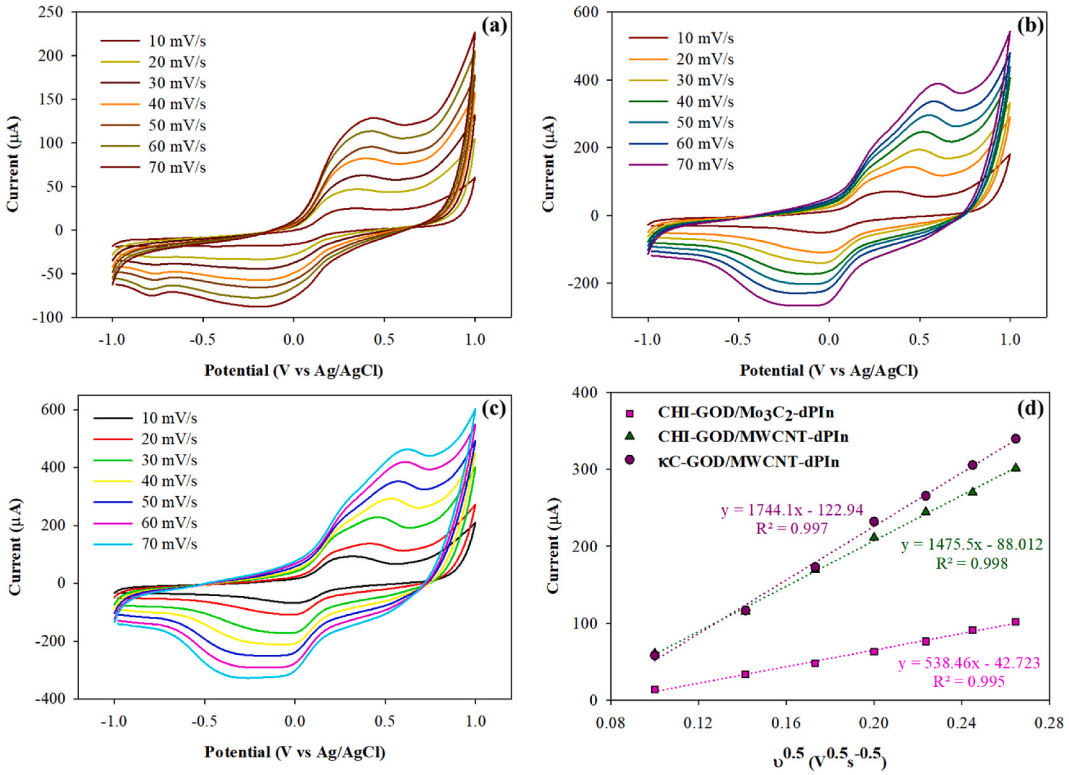

Fig. 4. Cyclic voltammograms at different scan rates in electrolyte solution containing 5 mM of $K_3[Fe(CN)_6]/K_4[Fe(CN)_6]$ and 0.1 M PBS in 0.1 M KCl of: (a) CHI-GOD/Mo_3C_2-dPIn; (b) CHI-GOD/MWCNT-dPIn; (c) κC-GOD/MWCNT-dPIn; and (d) the anodic current responses at various square root of scan rates of the modified electrodes.

3.4. Chronoamperometric measurement

Chronoamperometric current response was measured in 0.1 M PBS solutions containing different glucose concentrations. The anodic potential applied was at +0.6 V vs Ag/AgCl to detect the H_2O_2 oxidation. The chronoamperometric current response vs. time for each glucose concentration and calibration curve of the various fabricated glucose sensors are revealed in Fig. 5(a-f). The current response tends to increase with increasing glucose concentration because H_2O_2 is oxidized at the electrode surface under applied +0.6 V vs Ag/AgCl and releases electrons leading to the increment in the current response [65]. The slope of the calibration curve (μA/mM) of divided by geometric surface area (cm^2) is normally referred to as the sensitivity of glucose sensors [66,67]. The linear regression equation of the CHI-GOD/Mo_3C_2-dPIn is $I = 0.2473C + 3.236$, $R^2 = 0.997$ equation (3) within the glucose concentration range of 2.5–10 mM with 1.03 % RSD of slope, and $I = 0.0178C + 5.599$, $R^2 = 0.996$ equation (4) within the glucose concentration range of 10–100 mM with 0.84 % RSD of slope; thus, its sensitivity values are 3.53 μA mM^{-1} cm^{-2} and 0.254 μA mM^{-1} cm^{-2}, respectively. However, the CHI-GOD/Mo_3C_2-dPIn is not appropriate for use in the glucose concentration range of 10–100 mM because the sensitivity is lower than the minimum sensitivity value required for a suitable blood glucose sensor (1 μA mM^{-1} cm^{-2}) [68]. The linear regression equation of the CHI-GOD/MWCNT-dPIn is $I = 1.3197C + 12.333$, $R^2 = 0.991$ equation (5) within the glucose concentration range of 0.5–25 mM with 2.16 % RSD of slope, and $I = 0.2398C + 38.608$, $R^2 = 0.994$ (equation 6) within the glucose concentration range of 25–75 mM with 3.35 % RSD of slope; thus, its sensitivity values are 18.85 μA mM^{-1} cm^{-2} and 3.43 μA mM^{-1} cm^{-2}, respectively. The linear regression equation of the κC-GOD/MWCNT-dPIn is $I = 1.1061C + 12.071$, $R^2 = 0.992$ (equation 7) within the glucose concentration range of 0.1–50 mM with 0.8 % RSD of slope; thus, its sensitivity value is 15.80 μA mM^{-1} cm^{-2}. Above 50 mM of glucose concentration, the current response tends to reach equilibrium. The sensitivity values of the CHI-GOD/MWCNT-dPIn and the κC-GOD/MWCNT-dPIn are higher than the lowest sensitivity value required for a blood glucose sensor, indicating that these sensors have a possibility for applying as a blood glucose sensor [68].

From the sensitivity values, it is evident that the glucose sensor fabricated from MWCNT-dPIn produces the higher glucose response than that of Mo_3C_2-dPIn. This is because MWCNT-dPIn allows the higher electron transfer than Mo_3C_2-dPIn, as confirmed by the higher redox current response as shown in Fig. 2, and the larger electroactive surface area (54.0 mm^2 for MWCNT-dPIn and 31.3 mm^2 for Mo_3C_2-dPIn) rendering the higher glucose oxidation. The κC-GOD/MWCNT-dPIn provides the wider linear glucose level range than the CHI-GOD/MWCNT-dPIn possibly because of the larger electroactive surface area; 39.9 mm^2 for the CHI-GOD/MWCNT-dPIn and 49.9 mm^2 for the κC-GOD/MWCNT-dPIn. The differences in sensing performance of the glucose sensor, as fabricated by the two different biopolymers as the support materials for enzyme immobilization, occur as they are different in chemical structures resulting

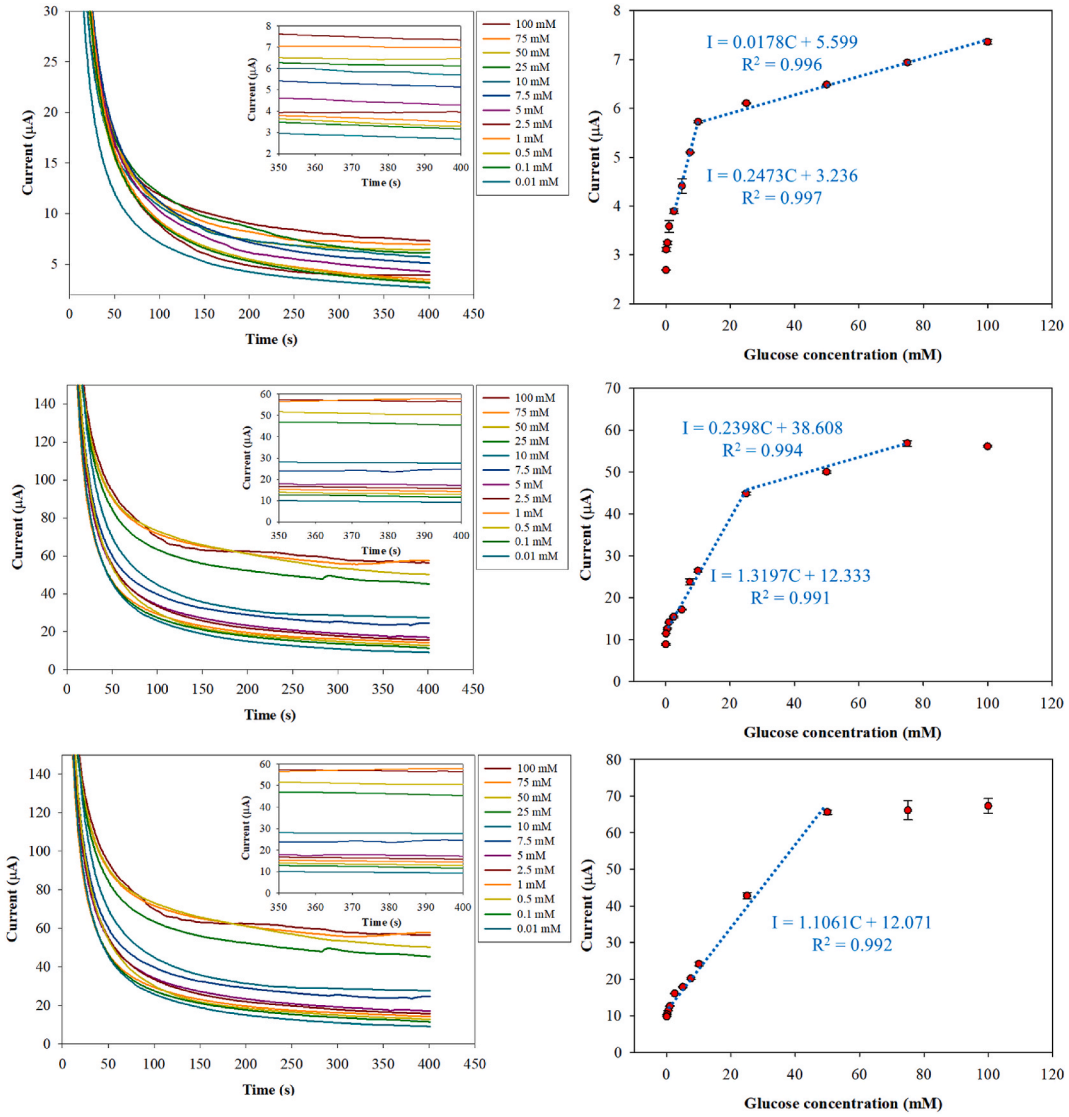

Fig. 5. Chronoamperometric current responses vs time and calibration curves of: (a) and (b) CHI-GOD/Mo_3C_2-dPIn; (c) and (d) CHI-GOD/MWCNT-dPIn; and (e) and (f) κC-GOD/MWCNT-dPIn.

in different enzyme interactions and film surface formations.

The continuous glucose responses of the fabricated glucose sensors in glucose solutions (0.01 mM–100 mM) are shown in Fig. S8. It can be seen that the glucose sensor fabricated from MWCNT-dPIn produces a higher glucose response than that of Mo_3C_2-dPIn. On the other hand, the glucose response of the κC-GOD/MWCNT-dPIn is higher than that of the CHI-GOD/MWCNT-dPIn. The continuous glucose responses shown illustrate that the fabricated glucose sensors are potentially suitable to utilize as continuous glucose sensors in real time application.

The limit of detection (LOD) is defined as the lowest amount of analyte in sample which can be detected but not necessarily quantitated under stated experimental conditions [69]. Herein, LOD was calculated by $3.3SD_b$/slope where SD_b is standard deviation of blank response and the slope is obtained from the linear response of the calibration curve. The calculations of LOD are reported in Table S6. The calculated LOD values of the CHI-GOD/Mo_3C_2-dPIn, the CHI-GOD/MWCNT-dPIn, and the κC-GOD/MWCNT-dPIn are 1574 μM, 115 μM and 30 μM, respectively.

3.5. Glucose sensor mechanism

The mechanism of glucose response in this work is related to the enzymatic reaction between GOD and glucose as presented in Scheme 1(B). First, glucose oxidation is catalyzed by GOD in which the glucose is oxidized by GOD-FAD to produce gluconolactone and GOD-$FADH_2$ as in the reaction (1) [70]. Gluconolactone reacts with water to generate gluconic acid as in the reaction (2). GOD-$FADH_2$

is re-oxidized by oxygen in order to reproduce GOD-FAD and generates H_2O_2 as in the reaction (3). Glucose detection can be measured by the H_2O_2 generation and O_2 consumption during the enzymatic reaction as the glucose concentration is directly proportional to H_2O_2 generation and O_2 consumption. Herein, the glucose detection is focused on the direct measurement of H_2O_2 generation via the investigation of the H_2O_2 oxidation at the anodic potential of +0.6 V vs Ag/AgCl as in the reaction (4). The MXene-dPIn and MWCNT-dPIn composites act as the electron acceptors from the reactions to electrode as in the reaction (5). These reactions (1–4) are referred to as in previous reports [14,71]. The existence of H_2O_2 can be proved by using the chromogenic oxygen acceptor (o-dianisidine) in the presence of peroxidase enzyme [14,71]. The color of the glucose solution incubated on the modified sensors for 10 min changed from colorless to brown as shown in Fig. S9. This result confirms that the mechanism of the fabricated glucose sensors involves in the generation of H_2O_2 [14,71].

$$\text{Glucose} + \text{GOD-FAD} \rightarrow \text{Gluconolactone} + \text{GOD-FADH}_2 \quad (1)$$

$$\text{Gluconolactone} + H_2O \rightarrow \text{Gluconic acid} \quad (2)$$

$$\text{GOD-FADH}_2 + O_2 + 2e^- + 2H^+ \rightarrow H_2O_2 + \text{GOD-FAD} \quad (3)$$

$$H_2O_2 \xrightarrow{+0.6\ \text{V vs Ag/AgCl}} O_2 + 2e^- + 2H^+ \quad (4)$$

$$\text{X-dPIn}^{2+} + 2e^- \rightarrow \text{X-dPIn (X is MXene or MWCNT.)} \quad (5)$$

The nature of the electrochemical reaction at the electrode surface was examined in a 10 mM glucose solution by cyclic voltammetry at the applied potential from −0.8 to 0.8 V at various scan rates. The cyclic voltammograms of various fabricated glucose sensors are shown in Fig. 6 (a-c) and the logarithmic relation between the anodic currents (I_{pa}) and the scan rates (υ) are shown in Fig. 6(d). The slope values of the logarithmic relation of I_{pa} vs. υ of the CHI-GOD/Mo_3C_2-dPIn and CHI-GOD/MWCNT-dPIn are 1.193, 1.1091, respectively. These values are close to 1 indicating that the electrochemical reaction at the electrode surface is the adsorption-controlled reaction [72]. For κC-GOD/MWCNT-dPIn, the slope of the logarithmic relation of I_{pa} vs. υ is 0.8625 $\mu A m V^{-1} s^{-1}$, the slope is in the range of 0.5–1 indicating the concurrently controlled adsorption and diffusion [72,73].

3.6. Glucose sensor performances

Glucose sensor selectivity was examined and illustrated by chronoamperometry at +0.6 V vs Ag/AgCl in a 10 mM glucose solution

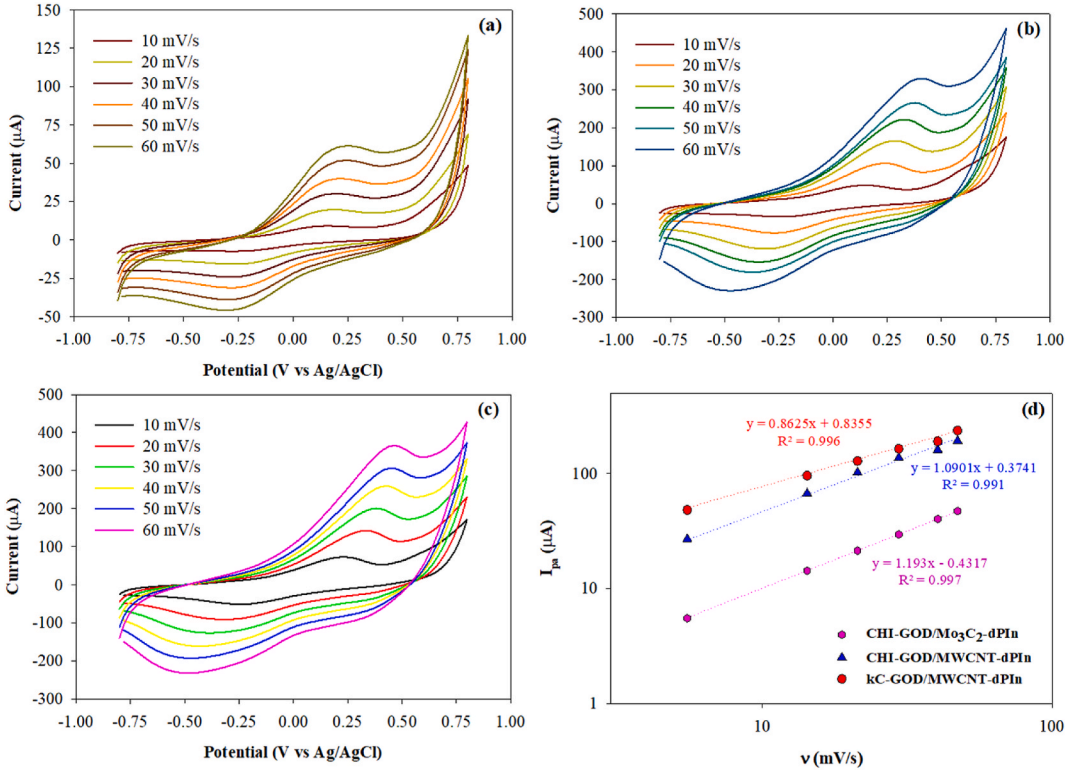

Fig. 6. Cyclic voltammograms at different scan rates in 10 mM glucose solution of: (a) CHI-GOD/Mo_3C_2-dPIn; (b) CHI-GOD/MWCNT-dPIn; (c) κC-GOD/MWCNT-dPIn; and (d) the logarithmic relation of anodic currents and scan rates.

mixed with 0.1 mM interferences of ascorbic acid (AA), uric acid (UA), lactic acid (LA), potassium chloride (KCl), and sodium chloride (NaCl). The current responses of pure glucose and glucose mixed interferences are shown in Fig. 7(a). The percentages of current response change of the glucose solutions mixed with the interferences are less than 8 % for CHI-GOD/Mo_3C_2-dPIn, 11 % for CHI-GOD/MWCNT-dPIn, and 12 % for κC-GOD/MWCNT-dPIn. The current response changes toward the interferences are about 10 % providing the superior glucose selectivity [66].

The reproducibility of the glucose sensors was investigated to verify the precision and accuracy of the response of the fabricated glucose sensor. The glucose sensors were fabricated with the same previous methods and then tested in a 10 mM glucose solution. The current responses of 7 fabricated glucose sensors are presented in Fig. 7(b). The percentages of the relative standard deviation (RSD = SD/mean) are 4.23 %, 1.17 %, and 1.23 % for CHI-GOD/Mo_3C_2-dPIn, CHI-GOD/MWCNT-dPIn, and κC-GOD/MWCNT-dPIn, respectively. The reproducibility of the fabricated glucose sensors is less than 5 %RSD indicating excellent reproducibility [74].

The repeatability of the glucose sensors was analyzed in a 10 mM glucose solution with the same electrode under the same conditions as shown in Fig. 7(c). The sensors were rinsed with deionized water after the glucose detection and dried at room temperature before reuse. The current responses tend to strongly decrease after the glucose sensor was reused in 2nd and 3rd cycles. This suggests that the biosensors should be disposable after the first use.

The long-term stability of the glucose sensors was examined in 10 mM glucose solution every 7 days, in which the glucose sensors were stored at 4 °C in vacuum sealed bags prior to use. The current signals of the fresh glucose sensors tested every 7 days are illustrated in Fig. 7(d). The current responses of CHI-GOD/Mo_3C_2-dPIn, CHI-MWCNT-dPIn, and κC-GOD/MWCNT-dPIn at 28 days of storage time are 77.0 %, 93.6 %, 93.2 %, respectively. The decrease in the current response is due to the enzyme leaching and the composite degradation during storage leading to a decrease in its conductivity [10]. The current signal of the glucose sensor based on MWCNT-dPIn is more stable than Mo_3C_2-dPIn possibly owing to the strong interaction between MWCNT and dPIn via the π-π interaction. The uses of CHI and κC as the support materials for the GOD immobilization provided the same sensor stability of ~93 % within 28 days. The summarized performances of the fabricated chronoamperometric glucose sensors were also tabulated in Table S5 in Supplementary Material.

3.7. *Effect of MWCNT content and continuous glucose response*

The effect of MWCNT content on the sensors was investigated at various MWCNT concentrations from 2 mg/mL to 12 mg/mL in the mixing with the dPIn solution at the volume ratio of 1:1. Cyclic voltammograms of MWCNT-dPIn at various concentrations of MWCNT solution are presented in Fig. S10(a). The results clearly indicate that the suitable concentration of MWCNT solution is 10 mg/mL

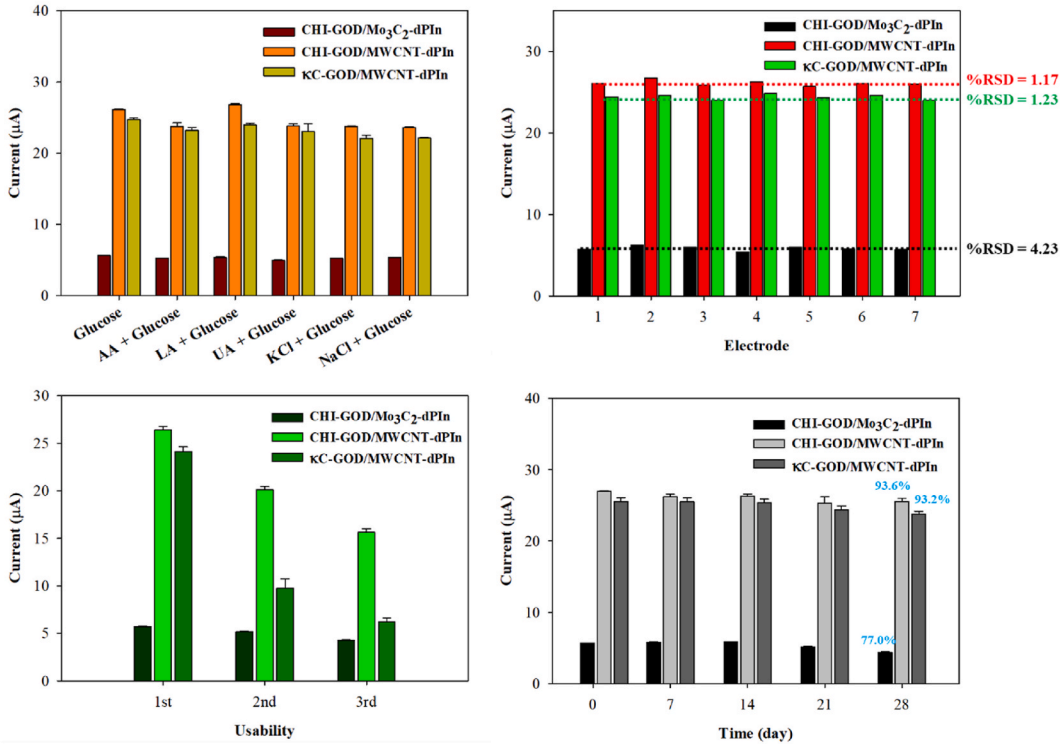

Fig. 7. Sensor performances: (a) selectivity (0.1 mM interferences in 10 mM glucose); (b) reproducibility; (c) repeatability; and (d) stability, in which (b)–(d) tested in 10 mM of glucose solution.

because the highest redox current response is obtained. A higher concentration of MWCNT might result in an excessive thickness of the coating layer leading to the blocking of the electron transfer from the $Fe(CN)_6]^{3-}$/$[Fe(CN)_6]^{4-}$ redox probe to the working electrode. The effect of MWCNT concentrations on the continuous glucose response is also shown in Fig. S10(b). The results illustrate that the glucose response increases with increasing concentrations of MWCNT solution up to 10 mg/mL of MWCNT solution, then the glucose response decreases at 12 mg/mL. This result is consistent with the decrease in redox current response from the cyclic voltammograms of Fig. S10(a). At an excessive concentration of MWCNT, the electron transfer efficiency decreases due to the excessively thick coating layer.

3.8. Comparison of enzymatic glucose sensors designed with conductive polymer composites/hybrids

The comparisons of sensitivity, LOD, and linear range of glucose level for enzymatic glucose sensors based on conductive polymer composites and hybrids are tabulated in Table 1. The sensitivity values of the present glucose sensors CHI-GOD/MWCNT-dPIn and the κC-GOD/MWCNT-dPIn are lower than the previous glucose sensors fabricated from Nf-GOD/fMWCNTs-PPy, GOD/PAN/PANI/Graphene, and GQD-GOD/PEDOT: PSS/Ti_3C_2, but higher than GOD/PPy-HRP-FCA, GOx-CHI/PPy-Au NPs, PPy/GOD/SWCNTs-$PhSO_3^{-1}$/PB, GOD/AuNPs: MWCNT: PANI, GOD/GP/PB/PPy. However, the sensitivity value is higher than the lowest sensitivity value required for a blood glucose sensor (1 μA mM^{-1} cm^{-2}) [68], which suggests that the presently fabricated glucose sensors provide sufficiently high responses to detect glucose. The calculated LOD values are 115 μM for the CHI-GOD/MWCNT-dPIn and 30 μM for the κC-GOD/MWCNT-dPIn. Although the calculated LODs are higher than some previous works, the present glucose sensors the CHI-GOD/MWCNT-dPIn and the κC-GOD/MWCNT-dPIn provide wider linear glucose ranges over the previous works. The linear range of glucose completely covers the requirements of glucose detection in blood (2.2–38.9 mM) [66], urine (2.78 mM and over 5.55 mM), and sweat (0.01–1 mM) [3]. For the fabricated glucose sensor based on CHI-GOD/Mo_3C_2-dPIn, the sensitivity value is relatively low (3.53 μA mM^{-1} cm^{-2}) in the linear range of 2.5–10 mM with the calculated LOD of 1574 μM. However, its sensitivity is higher than the lowest sensitivity value required for a blood glucose sensor. Herein, the advantage of the glucose sensors fabricated on SPCE is of a practical use as the SPCE consists of the three-electrodes cell consisting of the working electrode, reference electrode (Ag/AgCl), and counter electrode. The glucose sensor can be fabricated on SPCE by the drop coating with MWCNT-dPIn and coated with an enzyme-biopolymer. Moreover, the glucose detection method is fast, as the electrochemical detection by chronoamperometry is a very facile detection method used for glucose sensors. The novelty of this work is the comparison of the composite materials between the Mo_3C_2-dPIn and the MWCNT-dPIn composites for increasing electrical signal and electroactive surface area and the different biopolymers (chitosan and κ-carrageenan) as the support materials for the enzyme immobilization.

4. Conclusions

The enzymatic glucose sensors as fabricated from MXene/dPIn and MWCNT-dPIn were systematically compared. Herein, MXene was molybdenum carbide (Mo_3C_2). The difference in morphology was observed by FE-SEM; Mo_3C_2-dPIn was of small particles of dPIn mixed with MXene, whereas MWCNT-dPIn was fibers of MWCNT fully covered with dPIn. The electrochemical behavior was investigated by CV and EIS, showing that MWCNT provided the higher redox current response and lower charge transfer resistance when compared to Mo_3C_2-dPIn, as MWCNT-dPIn possessed the higher electrical conductivity than Mo_3C_2/dPIn. Moreover, the electrochemical surface area of MWCNT-dPIn (54.0 mm^2) was larger than Mo_3C_2-dPIn (31.3 mm^2), consistent with the morphological surfaces of the materials. The biopolymer types between chitosan (CHI) and κ-carrageenan (κC) were compared for using as the support matrix for the GOD enzyme immobilization. The results illustrated that the electroactive surface area of the κC-GOD/MWCNT-dPIn (49.9 mm^2) was higher than the CHI-GOD/MWCNT-dPIn (39.9 mm^2), resulting in the increases in enzymes immobilization and higher enzymatic reaction toward glucose. The glucose response was investigated by chronoamperometry. The CHI-GOD/MWCNT-dPIn possessed the higher sensitivity and wider glucose detection range than the CHI-GOD/Mo_3C_2-dPIn, confirming that the glucose response of the CHI-GOD/MWCNT-dPIn was superior to that of CHI-GOD/Mo_3C_2-dPIn. The κC-GOD/MWCNT-dPIn showed the widest glucose concentration range from 0.1 mM to 50 mM with sensitivity of 15.80 μA mM^{-1} cm^{-2} and the calculated LOD was 30 μM. The fabricated glucose sensors were of high selectivity, high stability at 93 % within 28 days, and good reproducibility for a disposable single use.

Data availability statement

Data will be made available on request.

CRediT authorship contribution statement

Katesara Phasuksom: Writing - original draft, Visualization, Validation, Methodology, Investigation, Formal analysis, Data curation, Conceptualization. **Nuttha Ariyasajjamongkol:** Methodology, Formal analysis. **Anuvat Sirivat:** Writing - review & editing, Supervision, Funding acquisition.

Declaration of competing interest

The authors declare that they have no known competing financial interests or personal relationships that could have appeared to

Table 1
Comparison of enzymatic glucose sensors designed with conductive polymer composites/hybrids.

Design glucose biosensor	Detection method	Electrode	Sensitivity ($\mu A \cdot mM^{-1} \cdot cm^{-2}$)	LOD	Linear range (mM)	Ref.
GOD/PPy-HRP-FCA	CA	composite carbon electrode	1.11	10 μM	0.08–1.3	[75]
GOx-CHI/PPy-Au NPs	CA	Glassy carbon	0.58	68 μM	1.0–20.0	[76]
PPy/GOD/SWCNTs-$PhSO_3^{-1}$/PB	CA	Platinum	6.0	10 μM	0.02–6.0	[77]
GOD/AuNPs: MWCNT: PANI	CV	Glassy carbon	12.73	–	2.0–12.0	[78]
Nf- GOD/fMWCNTs-PPy	CA	Platinum	54.2	5.0 μM	0.05–4.1	[16]
GOD/GP/PB/PPy	CA	Graphite rod	1.9	100 μM	0.1–20.0	[79]
GOD/PEDOT/CF	CA	Carbon fiber microelectrode	8.5	–	0.5–15.0	[80]
GQD- GOD/PEDOT: PSS/Ti_3C_2	DPV	SPCE	21.64	65 μM	0–0.5	[81]
GOD/PEDOT: SCX/MXene	CA	Glassy carbon	–	22.5 μM	0.5–8.0	[82]
GOD/PAN/PANI/Graphene	CA	Platinum disk	29.11	2.10 μM	0.01–1.97	[83]
CHI-GOD/Mo_3C_2-dPIn	CA	SPCE	3.53	1574 μM	2.5–10.0	**This work**
CHI-GOD/MWCNT-dPIn	CA	SPCE	18.85	115 μM	0.5–25.0	
κC-GOD/MWCNT-dPIn	CA	SPCE	15.80	30 μM	0.1–50.0	

CA is chronoamperometry. CV is cyclic voltammetry. DPV is differential pulse voltammetry. LODs are calculated values.

influence the work reported in this paper.

Acknowledgements

The authors particularly grateful for the assistance and financial supports from the Conductive and Electroactive Polymers Research Unit, and the Ratchadapisek Somphot Fund for Postdoctoral Fellowship, and the Thailand Science Research and Innovation Fund (TSRI-CU), all of Chulalongkorn University; and the National Research Council of Thailand (NRCT).

Appendix A. Supplementary data

Supplementary data to this article can be found online at doi:mmcdoino.

References

[1] V.S. Reddy, B. Agarwal, Z. Ye, C. Zhang, K. Roy, A. Chinnappan, R.J. Narayan, S. Ramakrishna, R. Ghosh, Recent advancement in biofluid-based glucose sensors using invasive, minimally invasive, and non-invasive technologies: a review, Nanomaterials 12 (2022) 1082.
[2] C. Heyser, R. Schrebler, P. Grez, New route for the synthesis of nickel (II) oxide nanostructures and its application as non-enzymatic glucose sensor, J. Electroanal. Chem. 832 (2019) 189–195.
[3] D. Bruen, C. Delaney, L. Florea, D. Diamond, Glucose sensing for diabetes monitoring: recent developments, Sensors 17 (2017) 1866.
[4] S. Radhakrishnan, S. Lakshmy, S. Santhosh, N. Kalarikkal, B. Chakraborty, C.S. Rout, Recent developments and future perspective on electrochemical glucose sensors based on 2D materials, Biosensors 12 (2022) 467.
[5] J. Kim, A.S. Campbell, J. Wang, Wearable non-invasive epidermal glucose sensors: a review, Talanta 177 (2018) 163–170.
[6] W. Villena Gonzales, A.T. Mobashsher, A. Abbosh, The progress of glucose monitoring—a review of invasive to minimally and non-invasive techniques, devices and sensors, Sensors, Sensors 19 (2019) 800.
[7] E. Costa-Rama, M.T. Fernández-Abedul, Paper-based screen-printed electrodes: a new generation of low-cost electroanalytical platforms, Biosensors 11 (2021) 51.
[8] R.A.S. Couto, J.L.F.C. Lima, M.B. Quinaz, Recent developments, characteristics and potential applications of screen-printed electrodes in pharmaceutical and biological analysis, Talanta 146 (2016) 801–814.
[9] E. Witkowska Nery, M. Kundys, P.S. Jeleń, M. Jönsson-Niedziółka, Electrochemical glucose sensing: is there still room for improvement? Anal. Chem. 88 (2016) 11271–11282.
[10] J. Lai, Y. Yi, P. Zhu, J. Shen, K. Wu, L. Zhang, J. Liu, Polyaniline-based glucose biosensor: a review, J. Electroanal. Chem. 782 (2016) 138–153.
[11] X. Lu Dhanjai, L. Wu, J. Chen, Y. Lu, Robust single-molecule enzyme nanocapsules for biosensing with significantly improved biosensor stability, Anal. Chem. 92 (8) (2020) 5830–5837.
[12] A. Müsse, F. La Malfa, V. Brunetti, F. Rizzi, M. De Vittorio, Flexible enzymatic glucose electrochemical sensor based on polystyrene-gold electrodes, Micromachines 12 (2021) 805.
[13] D.D. Borole, U.R. Kapadi, P.P. Mahulikar, D.G. Hundiwale, Conducting polymers: an emerging field of biosensors, Des. Monomers Polym. 9 (2006) 1–11.
[14] K. Phasuksom, A. Sirivat, Chronoampermetric detection of enzymatic glucose sensor based on doped polyindole/MWCNT composites modified onto screen-printed carbon electrode as portable sensing device for diabetes, RSC Adv. 12 (2022) 28505–28518.
[15] M.I. Pilo, S. Baluta, A.C. Loria, G. Sanna, N. Spano, Poly(thiophene)/graphene oxide-modified electrodes for amperometric glucose biosensing, Nanomaterials 11 (2021) 2890.
[16] B.K. Shrestha, R. Ahmad, S. Shrestha, C.H. Park, C.S. Kim, Globular shaped polypyrrole doped well-dispersed functionalized multiwall carbon nanotubes/nafion composite for enzymatic glucose biosensor application, Sci. Rep. 7 (2017) 16191.
[17] K. Ma, A. Sinha, X. Dang, H. Zhao, Electrochemical preparation of gold nanoparticles-polypyrrole Co-decorated 2D MoS_2 nanocomposite sensor for sensitive detection of glucose, J. Electrochem. Soc. 166 (2) (2019) B147–B154.

[18] G. Bagdžiūnas, D. Palinauskas, Poly(9H-carbazole) as a organic semiconductor for enzymatic and non-enzymatic glucose sensors, Biosensors 10 (2020) 104.
[19] F. Jiménez-Fiérrez, M.I. González-Sánchez, R. Jiménez-Pérez, J. Iniesta, E. Valero, Glucose biosensor based on disposable activated carbon electrodes modified with platinum nanoparticles electrodeposited on poly(Azure A), Sensors 20 (2020) 4489.
[20] L. Kumar, R. Gupta, D. Thakar, V. Vibhu, S. Annapoorni, A new route to glucose sensing based on surface plasmon resonance using polyindole, Plasmonics 8 (2013) 487–494.
[21] V. Nirbhaya, C. Chaudhary, D. Chauhan, R. Chandra, S. Kumar, Multiwalled carbon nanotube nanofiller-polyindole polymer matrix-based efficient biosensor for the rapid detection of swine flu, New J. Chem. 46 (2022) 6201–6211.
[22] A. Thadathil, H. Pradeep, D. Joshy, Y.A. Ismail, P. Periyat, Polyindole and polypyrrole as a sustainable platform for environmental remediation and sensor applications, Mater. Adv. 3 (2022) 2990–3022.
[23] W. Lei, W. Si, Y. Xu, Z. Gu, Q. Hao, Conducting polymer composites with graphene for use in chemical sensors and biosensors, Microchim. Acta 181 (2014) 707–722.
[24] S. Baig, R. T subramaniam, K. ramish, A. Numan, J. Iqbal, Conducting polymer composites in electrochemical sensors, in: V. Mittal (Ed.), Conducting Polymer Composites, Central West Publishing Australia, 2019 chap. (chapter 2).
[25] Z. Wang, Z. Dai, Carbon nanomaterial-based electrochemical biosensors: an overview, Nanoscale 7 (2015) 6420–6431.
[26] W.-J. Guan, Y. Li, Y.-Q. Chen, X.-B. Zhang, G.-Q. Hu, Glucose biosensor based on multi-wall carbon nanotubes and screen printed carbon electrodes, Biosens. Bioelectron. 21 (2005) 508–512.
[27] A. Sinha, Dhanjai, H. Zhao, Y. Huang, X. Lu, J. Chen, R. Jain, MXene: an emerging material for sensing and biosensing, TrAC, Trends Anal. Chem. 105 (2018) 424–435.
[28] A. Sinha, K. Ma, H. Zhao, 2D Ti(3)C(2)T(x) flakes prepared by in-situ HF etchant for simultaneous screening of carbamate pesticides, J. Colloid Interface Sci. 590 (2021) 365–374.
[29] J. Yoon, M. Shin, J. Lim, J.-Y. Lee, J.-W. Choi, Recent advances in MXene nanocomposite-based biosensors, Biosensors 10 (2020) 185.
[30] X. Wu, P. Ma, Y. Sun, F. Du, D. Song, G. Xu, Application of MXene in electrochemical sensors: a review, Electroanalysis 33 (2021) 1827–1851.
[31] A. Sinha, Dhanjai, S.M. Mugo, J. Chen, K.S. Lokesh, 14 - MXene-based sensors and biosensors: next-generation detection platforms, in: C. Mustansar Hussain (Ed.), Handbook of Nanomaterials in Analytical Chemistry, Elsevier, 2020, pp. 361–372.
[32] Y. Ge, S. Ma, K. Bao, Q. Tao, X. Zhao, X. Feng, L. Li, B. Liu, P. Zhu, T. Cui, Superconductivity with high hardness in Mo_3C_2, Inorg. Chem. Front. 6 (2019) 1282–1288.
[33] Y. Nan, Z. Zhang, Z. Wang, H. Yuan, Y. Zhou, J. Wei, Controllable synthesis of Mo_3C_2 encapsulated by N-doped carbon microspheres to achieve highly efficient microwave absorption at full wavebands: from lemon-like to fig-like morphologies, Inorg. Chem. 61 (2022) 6281–6294.
[34] X. Zang, C. Shen, Y. Chu, B. Li, M. Wei, J. Zhong, M. Sanghadasa, L. Lin, Laser-induced molybdenum carbide–graphene composites for 3D foldable paper electronics, Adv. Mater. 30 (2018) 1800062.
[35] J. Zdarta, A.S. Meyer, T. Jesionowski, M. Pinelo, A general overview of support materials for enzyme immobilization: characteristics, properties, practical utility, Catalysts 8 (2018) 92.
[36] Y. Jiang, J. Wu, Recent development in chitosan nanocomposites for surface-based biosensor applications, Electrophoresis 40 (2019) 2084–2097.
[37] F.P. Ramanery, A.A.P. Mansur, H.S. Mansur, One-step colloidal synthesis of biocompatible water-soluble ZnS quantum dot/chitosan nanoconjugates, Nanoscale Res. Lett. 8 (2013) 512.
[38] Dhanjai, A. Sinha, Amperometric response characteristics of rabeprazole at N-doped CNTs-chitosan nanosensor in solubilized system, J. Electrochem. Soc. 164 (2017) H639–H646.
[39] J. Necas, L. Bartosikova, Carrageenan: a review, Vet. Med. 58 (2013) 187–205.
[40] I. Rassas, M. Braiek, A. Bonhomme, F. Bessueille, G. Raffin, H. Majdoub, N.A.-O. Jaffrezic-Renault, Highly sensitive voltammetric glucose biosensor based on glucose oxidase encapsulated in a chitosan/kappa-carrageenan/gold nanoparticle bionanocomposite, Sensors 19 (2019) 154.
[41] I. Rassas, M. Braiek, A. Bonhomme, F. Bessueille, G. Rafin, H. Majdoub, N. Jaffrezic-Renault, Voltammetric glucose biosensor based on glucose oxidase encapsulation in a chitosan-kappa-carrageenan polyelectrolyte complex, Mater. Sci. Eng. C 95 (2019) 152–159.
[42] Y. Xie, Z. Li, J. Zhou, Hamiltonian replica exchange simulations of glucose oxidase adsorption on charged surfaces, Phys. Chem. Chem. Phys. 20 (2018) 14587–14596.
[43] M. Dul, K.J. Paluch, H. Kelly, A.M. Healy, A. Sasse, L. Tajber, Self-assembled carrageenan/protamine polyelectrolyte nanoplexes—investigation of critical parameters governing their formation and characteristics, Carbohydr, Polym 123 (2015) 339–349.
[44] K. Phasuksom, A. Sirivat, Synthesis of nano-sized polyindole via emulsion polymerization and doping, Synth. Met. 219 (2016) 142–153.
[45] L. Zhou, Y. Jiang, J. Gao, X. Zhao, L. Ma, Graphene oxide as a matrix for the immobilization of glucose oxidase, Appl. Biochem. Biotechnol. 168 (2012) 1635–1642.
[46] G. Lawrie, I. Keen, B. Drew, A. Chandler-Temple, L. Rintoul, P. Fredericks, L. Grøndahl, Interactions between alginate and chitosan biopolymers characterized using FTIR and XPS, Biomacromolecules 8 (2007) 2533–2541.
[47] L.F. Ang, L.Y. Por, M.F. Yam, Study on different molecular weights of chitosan as an immobilization matrix for a glucose biosensor, PLoS One 8 (2013) e70597.
[48] I.S.E.A.M. Hezma, A. Rajeh, Mustafa Kamal, Spectroscopic and thermal properties of PU/PVC doped with multi-walled carbon nanotube, Der Pharma Chem. 8 (2016) 201–208.
[49] M. Şen, E.N. Erboz, Determination of critical gelation conditions of κ-carrageenan by viscosimetric and FT-IR analyses, Food Res. Int. 43 (2010) 1361–1364.
[50] S.A.-O. Derkach, N.G. Voron'ko, Y.A. Kuchina, Intermolecular interactions in the formation of polysaccharide-gelatin complexes: a spectroscopic study, Polymers 14 (2022) 2777.
[51] J. Fu, Z. Pang, J. Yang, F. Huang, Y. Cai, Q. Wei, Fabrication of polyaniline/carboxymethyl cellulose/cellulose nanofibrous mats and their biosensing application, Appl. Surf. Sci. 349 (2015) 35–42.
[52] V. Kathiresan, D. Thirumalai, T. Rajarathinam, M. Yeom, J. Lee, S. Kim, J.-H. Yoon, S.-C. Chang, A simple one-step electrochemical deposition of bioinspired nanocomposite for the non-enzymatic detection of dopamine, J. Anal. Sci. Technol. 12 (2021) 5.
[53] N. Aristov, A. Habekost, Cyclic voltammetry - a versatile electrochemical method investigating electron transfer processes, World J. Chem. Educ. 3 (2015) 115–119.
[54] K.K. Onchoke, A.D. Trevino, Electrochemical characteristics of benzanthrone studied via cyclic voltammetry: charge transfer redox processes, Anal. Chem. Lett. 9 (2019) 128–142.
[55] A. Muhammad, R. Hajian, N.A. Yusof, N. Shams, J. Abdullah, P.M. Woid, H. Garmestani, A screen printed carbon electrode modified with carbon nanotubes and gold nanoparticles as a sensitive electrochemical sensor for determination of thiamphenicol residue in milk, RSC Adv. 8 (2018) 2714.
[56] Y. Yuan, T. Li, Z. Ye, Y. Feng, Z. Chen, Y. Wang, Y. Sun, H. Wu, Z. Yang, Y. Wang, Y. Zhang, L. Huang, B. Liang, A one-step electropolymerized biomimetic polypyrrole membrane-based electrochemical sensor for selective detection of valproate, Front. Bioeng. Biotechnol. 10 (2022) 851692.
[57] S. Kadian, B.D. Arya, S. Kumar, S.N. Sharma, R.P. Chauhan, A. Srivastava, P. Chandra, S.P. Singh, Synthesis and application of PHT-TiO_2 nanohybrid for amperometric glucose detection in human saliva sample, Electroanalysis 30 (2018) 2793–2802.
[58] B.K. Shrestha, R. Ahmad, H.M. Mousa, I.-G. Kim, J.I. Kim, M.P. Neupane, C.H. Park, C.S. Kim, High-performance glucose biosensor based on chitosan-glucose oxidase immobilized polypyrrole/nafion/functionalized multi-walled carbon nanotubes bio-nanohybrid film, J. Colloid Interface Sci. 482 (2016) 39–47.
[59] H. Gul, A.-u.-H.A. Shah, S. Bilal, Achieving ultrahigh cycling stability and extended potential window for supercapacitors through asymmetric combination of conductive polymer nanocomposite and activated carbon, Polymers 11 (2019) 1678.
[60] G.N.H. Zare, M. Jahanshahi, M. Rahimnejad, Mohsen Rezvani, Highly stable biosensor based on glucose oxidase immobilized in chitosan film for diagnosis of diabetes, Rom, Biotechnol. Lett. 22 (2017) 12611–12619.
[61] C.-H. Hsu, A.K. Gupta, A. Purwidyantri, B.A. Prabowo, C.-H. Chen, C.-C. Chuang, Y.-C. Tian, Y.-J. Lu, C.-S. Lai, Sensing Alzheimer's disease utilizing Au electrode by controlling nanorestructuring, Chemosensors 10 (2022) 94.

[62] S. Jin, D.M. Porterfield, in: S. Pier Andrea Biosensors (Ed.), IntechOpen, Rijeka, 2011. Ch. 11.
[63] G.B.V.S. Lakshmi, A.K. Yadav, N. Mehlawat, R. Jalandra, P.R. Solanki, A. Kumar, Gut microbiota derived trimethylamine N-oxide (TMAO) detection through molecularly imprinted polymer based sensor, Sci. Rep. 11 (2021) 1338.
[64] J.A. Hondred, J.C. Breger, N.J. Alves, S.A. Trammell, S.A. Walper, I.L. Medintz, J.C. Claussen, Printed graphene electrochemical biosensors fabricated by inkjet maskless lithography for rapid and sensitive detection of organophosphates, ACS Appl. Mater. Interfaces 10 (2018) 11125–11134.
[65] R. Tipnis, F. Vaddiraju S Fau - Jain, D.J. Jain F Fau - Burgess, F. Burgess Dj Fau - Papadimitrakopoulos, F. Papadimitrakopoulos, Layer-by-layer assembled semipermeable membrane for amperometric glucose sensors, J. Diabetes Sci. Technol. 1 (2007) 193–200.
[66] S.A. Hashemi, S.M. Mousavi, S. Bahrani, S. Ramakrishna, Polythiophene silver bromide nanostructure as ultra-sensitive non-enzymatic electrochemical glucose biosensor, Eur. Polym. J. 138 (2020) 109959.
[67] W. Liu, X. Wu, X. Li, Gold nanorods on three-dimensional nickel foam: a non-enzymatic glucose sensor with enhanced electro-catalytic performance, RSC Adv. 7 (2017) 36744–36749.
[68] K.E. Toghill, R.G. Compton, Electrochemical non-enzymatic glucose sensors: a perspective and an evaluation, Int. J. Electrochem. Sci. 5 (2010) 1246–1301.
[69] A. Shrivastava, V. Gupta, Methods for the determination of limit of detection and limit of quantitation of the analytical methods, Chronicles Young Sci. 2 (2011) 21–25.
[70] P. Balla Dhanjai, A. Sinha, L. Wu, X. Lu, D. Tan, J. Chen, Co(3)O(4) nanoparticles supported mesoporous carbon framework interface for glucose biosensing, Talanta 203 (2019) 112–121.
[71] P. Krzyczmonik, E. Socha, S. Skrzypek, Electrochemical detection of glucose in beverage samples using poly(3,4-ethylenedioxythiophene)-modified electrodes with immobilized glucose oxidase, Electrocatalysis 9 (2018) 380–387.
[72] W.A. Adeosun, A.M. Asiri, H.M. Marwani, Sensitive determination of 2-nitrophenol using electrochemically deposited polymethyl red film for healthcare and environmental safety, Synth. Met. 261 (2020) 116321.
[73] Y. Zhou, W. Tang, J. Wang, G. Zhang, S. Chai, L. Zhang, T. Liu, Selective determination of dopamine and uric acid using electrochemical sensor based on poly (alizarin yellow R) film-modified electrode, Food Anal. Methods 6 (2014) 3474–3481.
[74] S.H. Lee, J.-H. Chung, H.-K. Park, G.-J. Lee, A Simple and facile glucose biosensor based on prussian blue modified graphite string, J. Sens. 2016 (2016) 1859292.
[75] F. Tian, G. Zhu, Bienzymatic amperometric biosensor for glucose based on polypyrrole/ceramic carbon as electrode material, Anal. Chim. Acta 451 (2002) 251–258.
[76] M. Şenel, Simple method for preparing glucose biosensor based on in-situ polypyrrole cross-linked chitosan/glucose oxidase/gold bionanocomposite film, Mater. Sci. Eng. C 48 (2015) 287–293.
[77] M. Raicopol, C.Prună A. Fau - Damian, L. Damian C Fau - Pilan, L. Pilan, Functionalized single-walled carbon nanotubes/polypyrrole composites for amperometric glucose biosensors, Nanoscale Res. Lett. 8 (2013) 316.
[78] R.K. Gangwar, V.A. Dhumale, K.S. Date, P. Alegaonkar, R.B. Sharma, S. Datar, Decoration of gold nanoparticles on thin multiwall carbon nanotubes and their use as a glucose sensor, Mater. Res. Express 3 (2016) 035008.
[79] A. Ramanavicius, A.I. Rekertaitė, R. Valiūnas, A. Valiūnienė, Single-step procedure for the modification of graphite electrode by composite layer based on polypyrrole, Prussian blue and glucose oxidase, Sensor. Actuator. B Chem. 240 (2017) 220–223.
[80] J. Chen, X. Zheng, Y. Li, H. Zheng, Y. Liu, S.-I. Suye, A glucose biosensor based on direct electron transfer of glucose oxidase on PEDOT modified microelectrode, J. Electrochem. Soc. 167 (2020) 067502.
[81] S.N. Nashruddin, J. Abdullah, M.A. Mohammad Haniff, M.H. Mat Zaid, O.P. Choon, M.F. Mohd Razip Wee, Label free glucose electrochemical biosensor based on poly(3,4-ethylenedioxy thiophene): polystyrene sulfonate/titanium carbide/graphene quantum dots, Biosensors 11 (2021) 267.
[82] P. Murugan, J. Annamalai, R.A.-O. Atchudan, M.A.-O. Govindasamy, D. Nallaswamy, D. Ganapathy, A.A.-O.X. Reshetilov, A.A.-O. Sundramoorthy, Electrochemical sensing of glucose using glucose oxidase/PEDOT:4-sulfocalix [4]arene/MXene composite modified electrode, Micromachines 13 (2022) 304.
[83] Y. Zupeng, The micro network of polyacrylonitrile (PAN)-polyaniline (Pani)-graphene (GRA) hybrid nanocomposites for effective electrochemical detection of glucose and improved stability, Int. J. Electrochem. Sci. 14 (2019) 3011–3023.